nature communications

Article

https://doi.org/10.1038/s41467-025-67598-4

Why covalent organic frameworks grow twisted on graphite

Received: 18 March 2025

Accepted: 4 December 2025

Published online: 13 December 2025

Check for updates

Veniero Lenzi, Karol Strutyński & Manuel Melle-Franco

Van der Waals 2D materials made of graphene and Covalent Organic Frameworks (COFs) show a large potential for advanced applications, such as in superconductive and twistronic devices. High-quality pyrene diboronic acid (PDBA) COFs have been recently achieved on graphite, showcasing highly reproducible twisted stackings and moiré superlattices. A fundamental understanding of the processes ruling the formation of these unexpected materials is yet lacking. Hereby, we address this issue by studying growing COFs at different twist angles with an ad-hoc hybrid molecular mechanics force field with near-DFT accuracy. This reveals that as PDBA COFs grow, the number of available thermodynamic minima decreases dramatically, which may effectively lock the COF in the unique twisted stacking found experimentally. In addition, the mobility on the surface is found to show large alterations with size and twist angle. We discuss how both findings are expected to play a fundamental role in the synthesis of twisted PDBA COFs monolayers on graphitic surfaces.

Covalent organic frameworks (COFs) are organic compounds covalently bonded into layered and 3D porous crystalline networks, which can be finely tuned by altering the molecular building blocks[1]. The porosity, large chemical diversity and tunability of COFs make them especially appealing for applications such as catalysis, sensing and optoelectronics[2]. With the advancement of chemical technologies, monolayer COFs on graphitic substrates[3,4] have been reported, opening the exciting possibility of combining the properties of graphene with the versatility and tunability of COFs. For instance, COF graphene heterostructures have been assembled to provide supercapacitors[5,6] and tunable photodetectors[7]. In addition, polyaromatic boronate ester COFs have been found to form paracrystalline films on carbon nanotubes with preferentially oriented pores[8]. Interestingly, as graphene and most COFs lattices are not commensurable, their mixture may naturally yield moiré heterostructures with exotic electronic properties[9]. Furthermore, COFs containing aromatic moieties, such as those assembled from pyrene diboronic acid (PDBA), exhibit interlayer π-π interactions, potentially leading to superconductive states or other nontrivial topological states[10]. The chemical production of high-quality graphene and COF heterostructures is highly desirable, as it should be more scalable compared to twisted graphene obtained by nanomanipulation[11]. In addition, if an aromatic-rich COF is paired with a twisted bilayer graphene (TBG), the electronic properties of the resulting material will be altered[12], potentially leading to COF-enhanced twistronic devices. In 2022, twisted PBDA-based 2D- COF layers were observed to naturally grow on a graphitic substrate at specific twist angles by in-situ Scanning Tunneling microscopy (STM), breaking the trigonal symmetry of both materials[4]. Recently, using the same technique, moiré COF superlattices were also demonstrated[13], showcasing how wet chemistry may be used to obtain twisted moiré materials. In this work, we aim to understand what drives the emergence of the twisting stacking of COFs observed on graphite.

From the seminal work of Bistritzer and MacDonald, who predicted flat bands on twisted bilayer graphene[14], computer modelling studies have been fundamental to the understanding of moiré systems[15]. However, the modelling of low-angle twisted systems implies large atomistic simulations. These limitations are more severe for graphene/COF heterostructures, whose lattice incommensurability, as well as the presence of a twist between layers, require model sizes which make ab initio methods unfeasible. Therefore, similarly to TBG, molecular mechanics (MM) models are the most suitable Hamiltonians to computationally investigate these materials.

Despite the availability of reliable atomistic models for COFs and graphene, to the best of our knowledge, a force field able to treat both

CICECO-Aveiro Institute of Materials, Department of Chemistry, University of Aveiro, Aveiro, Portugal. e-mail: manuelmelle@ua.pt

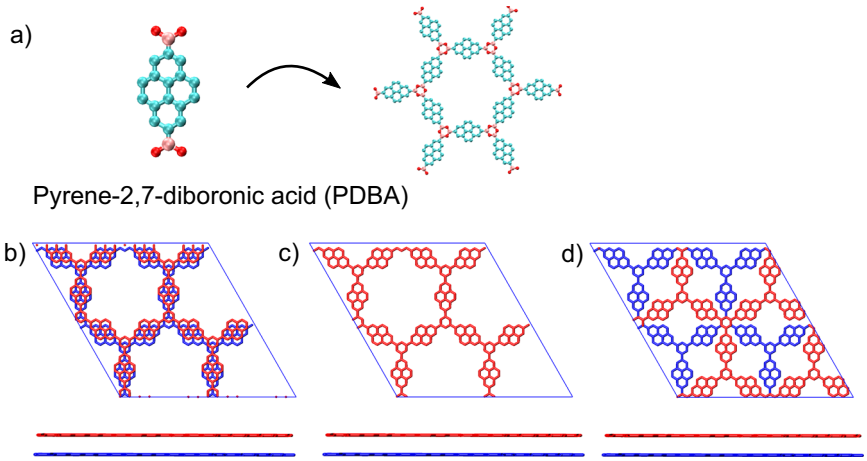

Fig. 1 | COF structure and stacking arrangements. a Representation of the PDBA monomer and COF, C atoms are cyan, B atoms are pink, and O atoms are red. PDBA COF bilayer with **b** parallel-displaced AA (pdAA) stacking, **c** eclipsed AA (eAA) stacking and **d** AB stacking. The two layers are rendered in blue and red. H atoms are omitted in all cases for clarity.

materials in a consistent way is not available. A number of classical force fields are available to model COFs[16–20] however, they commonly show reduced accuracy when compared with quantum methodologies. In fact, to improve on this, existing force fields have been reparametrized based on ab initio calculations[21,22]. De Vos and coworkers have recently reported a quantum-derived, yet fully classical, force field addressing a broad variety of COFs, termed ReDD-COFFEE (RC), yielding remarkable structural accuracy[23].

Due to the large interest in carbon materials, a substantial number of dedicated force fields have been developed over the years. These models are often able to accommodate carbon chemical bonding heterogeneity as well as, separately, intermolecular interactions, fitted for graphite and graphene[24]. As a matter of fact, most classical intermolecular potentials derived for organic systems, being isotropic, fail to reproduce the subtle, highly anisotropic interatomic interaction behind the sliding and rotation energetics of stacked graphene layers[25,26]. In fact, phenomenologically, this depends upon the interlayer registry, that is, the relative alignment between adjacent layers, which has to be explicitly considered in order to correctly account for the contact interactions in graphitic materials[27]. These interactions are fundamental to predict the stacking and, more generally, the local structures of the graphene layers on TBG systems[15,28]. Here, we selected the dihedral-angle-corrected registry-dependent interlayer potential (DRIP)[29] as it allows for an accurate, yet classical description of the interlayer interactions between graphene layers, outperforming previous potentials[30].

The combination of RC with DRIP, both of which are parametrised to mimic DFT results, allows for an accurate depiction of intermolecular interactions, yet with a modest computational effort suitable for large-scale calculations. This improves upon related recent studies of COFs on graphene[31], and metallic substrates[32], which, being focused on the growth dynamics, used a more generic depiction of the interactions with the underlying surfaces. The selected approach presents an improved representation of both the COF molecular structure and interfacial energetics, fundamental to understanding the appearance of twisted COFs on graphite. This methodology can be readily extended to any 2D-COF containing carbon polyaromatic moieties and other substrates, like, for instance, hexagonal boron nitride[33]. Yet, the explicit inclusion of solvents or other substrates would imply the development of specific parameters consistent with both force fields.

For the sake of completeness, it must be noted that machine-learned force fields have also been applied to investigate layered COF crystals[34] and graphene systems[35,36]. However, while being able to provide an accuracy comparable to density functional theory (DFT) calculations if trained properly, this kind of Hamiltonian is usually more computationally intensive than its classical counterparts[37] and was consequently considered not suitable for this study because of the twisted heterostructures modelled sizes, ranging from tens to hundreds of thousands of atoms.

Table 1 | Lattice parameters and binding energies for PDBA bilayers in different stacking arrangements computed with the RC force field and DFT

Quantity	RC force field	DFT
Lattice constant a,b	2.241 nm	2.247 nm
E_B (eAA)	−0.24 eV/pyr	−0.25 eV/pyr
E_B (pdAA)	−0.30 eV/pyr	−0.34 eV/pyr
E_B (AB)	−0.21 eV/pyr	−0.23 eV/pyr

Results and discussion

Model validation

DRIP has already been found to describe accurately the interlayer interactions as well as, in conjunction with intramolecular potentials, the geometric parameters of multilayer graphene and graphitic systems[29,30]. To validate the RC force-field model, we computed geometric parameters and binding energies of selected bulk and bilayer structures of the PDBA COF with different stacking arrangements and compared them with DFT results, Fig. 1. The force field yields lattice parameters within 0.5% of the DFT values, which yields PDBA COF lattice parameters with a 1.2 % mismatch with respect to graphene (a = b = 0.246 nm), Table 1.

At the DFT level, the most stable bilayer COF shows a parallel displaced AA (pdAA) stacking, with a displacement of 1.4 Å. This is followed by the eclipsed AA (eAA) stacking and the AB stacking, which is the least thermodynamically likely. The RC force field model reproduces well the ordering and the ratio between energies of the different stacking arrangements, Table 1. In order to quantitatively address the different twisted graphene/PDBA heterostructures, it is necessary to use a COF-graphene registry interaction potential, as this is a fundamental ingredient to model TBG systems. With this in mind, we adopted the DRIP scheme to treat the graphene-pyrene interactions, while all the other interlayer interactions were treated using the RC parameters. To evaluate the soundness of this approach, we

https://doi.org/10.1038/s41467-025-67598-4

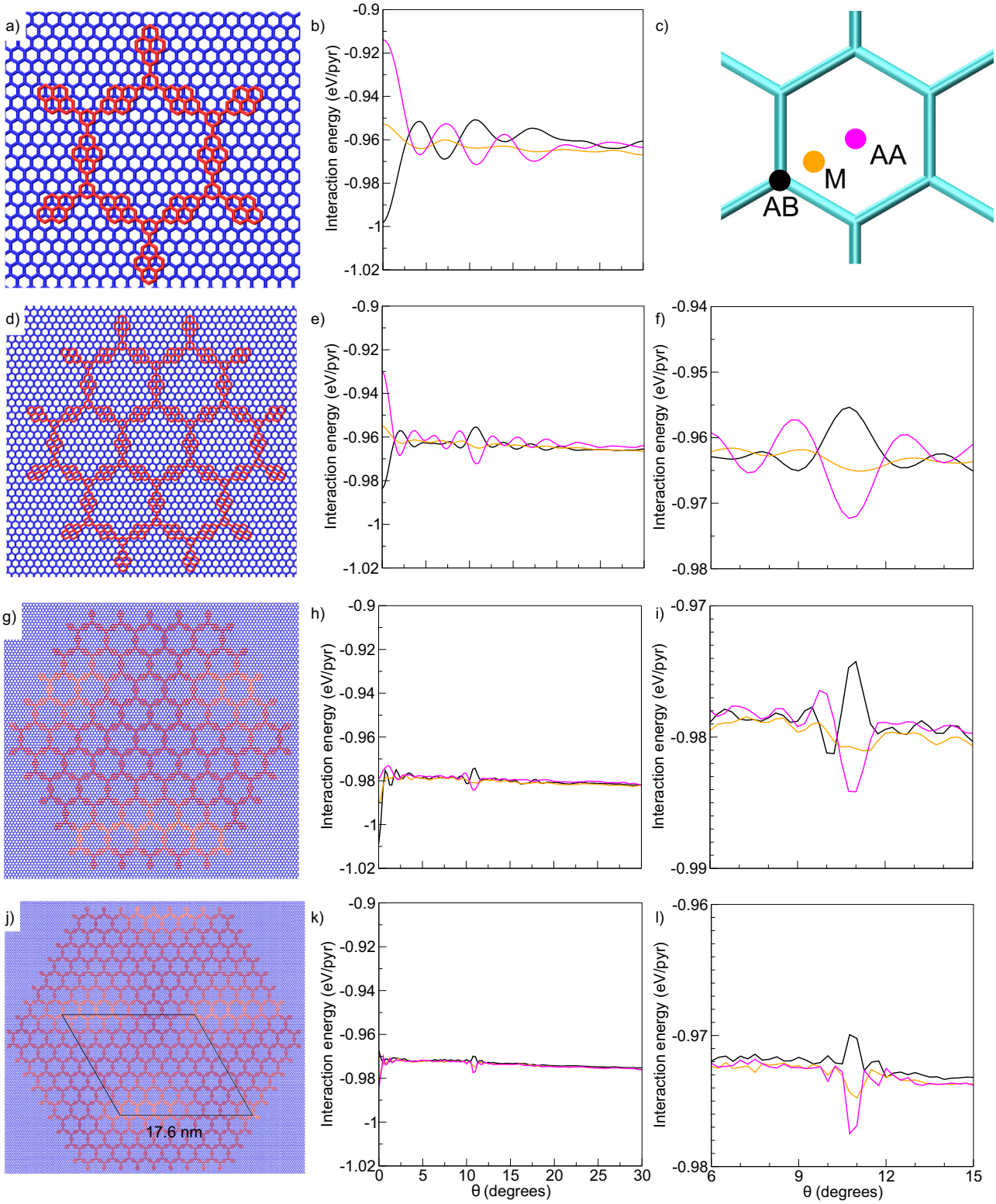

Fig. 2 | Stacking and twisting energetics on graphene. 12-pyr (**a**), 42-pyr (**d**), 240-pyr (**g**) and 756-pyr (**j**) PDBA COFs on graphene at the AB sampling point with zero twist and corresponding binding energies at different twist angles for 12-pyr (**b**), 42-pyr (**e**) 240-pyr (**h**) and 756-pyr (**k**), and zoomed region around 11 degrees for the 42-pyr (**f**), 240-pyr (**i**) and 756-pyr (**l**). **c** shows the labelling and color scheme for the three different sampling points on the graphene unit cell. Labels AA and AB highlight the stacking in the centermost area. For the 756-pyr COF (**j**), the moiré superlattice cell is highlighted.

computed the binding energy of a 12 pyr 2D-PDBA on graphene, and found a value of 1.00 eV/pyr and a G/COF distance of 3.40 Å. In comparison, DFT calculations of PDBA trimers on graphene yielded a binding energy of 1.11 eV/pyr and a G/COF distance of 3.48 Å, in good agreement with the hybrid RC/DRIP force field, indicating the latter is a suitable choice to quantitatively simulate PDBA COFs on graphene.To validate this approach, we compared the potential curves for MM and DFT of the rotational and sliding motions of a PDBA trimer on

graphene (Fig. S1). RC/DRIP shows a remarkable agreement with DFT. It recovers 92% of the DFT binding energy at the global minimum (0.98 eV/pyr, vs. 1.05 eV/pyr, respectively), and also yields a rather similar rotational behaviour for most angles. Regarding the sliding displacements, MM underestimates the maximum by 20% but otherwise compares favorably. It must be noted that the use of the pristine RC force field, Fig. S1, yields substantially flatter potential curves, severely underestimating the twisting and sliding barriers, thus confirming the need for accurate pyrene-graphene π-π interactions. As a whole, the hybrid RC/DRIP force field captures the intricacies of the graphene/COF interlayer interactions in good quantitative agreement with DFT in all relevant potential energy regions, supporting the application of this scheme for the energetics of twisted COFs on graphitic surfaces.

Twisting energetics

To understand the origin of the twist angles observed between PDBA COFs and the graphite substrate, we studied the binding energies of COFs on graphene at different twist angles. For this, we built PDBA COFs of increasing sizes, namely with 12, 42, 240 and 756 pyrenes, comprising respectively 330, 1164, 6690 and 21,114 atoms and diameters of 4.85 nm, 8.72 nm, 22.17 nm and 40.19 nm, Fig. 2, (a), (d), (g) and (j). Thus, representing values at, below, and above the experimentally derived critical size for PDBA COFs growth on graphite, 9 nm[4]. The COFs' center of mass were then positioned and twisted on three selected points on the graphene unit cell, Fig. 2(c); results with a full set of sampling points can be found in the Supplemental Information (SI)[29].

It is illustrative to comparatively analyze the effect of different sizes COFs on the stacking without twisting. 12-pyr COF shows Bernal stacking with graphene, Fig. 2(a), which is conserved in the central region of all systems. As we depart from the center, the stacking progressively moves out of phase reaching eclipsed stacking arrangements, as a consequence of the lattice mismatch. This reveals a moiré pattern with a periodicity of 17.6 nm appearing as periodic lighter areas on the representations of 240-pyr and 756-pyr COFs, Fig. S5, where the pyrene moieties and graphene are superposed and thus the ratio of white pixels is maximized.

When twisting is considered, a rich energy landscape is revealed. First, for the 12-pyr COF Fig. 2(b), the binding energy shows a clear dependence upon the registry between the COF and the substrate. In fact, the adsorption energies for untwisted systems, i.e. at 0 degrees, range between −1.00 and −0.91 eV/pyr, and the lowest energy is obtained for the AB sampling point, Fig. 2(c), which makes the pyrene moieties assume a graphitic Bernal-like stacking with respect to the substrate. As the twist angle increases, several equally spaced local minima appear at 7.5 and 14 degrees, showing periodic-like oscillation with increasing twist angles. Conversely, for the AA sampling point, the energy minimum is located at the twist angle of 11 degrees, with other higher energy minima appearing around 4 and 17 degrees. These features can be rationalised by the balance between eclipsed and Bernal-like π-π pyrene-graphene stackings at the different twist angles, Fig. S3, emphasising the necessity of a registry-dependent interlayer potential. Furthermore, similar results were obtained for 12-pyr on hexagonal boron nitride using an appropriate potential[38], Fig. S8, highlighting the potential generalizability of these findings and the approximations used.

By increasing the size to 42-pyr COF, Fig. 2(e), the energy-angle curves alter significantly. In this case, the fully aligned orientation is the lowest energy state for the AB sampling point only, while for the AA sampling point, the lowest energy is found now at 11 degrees, Fig. 2(f). The periodic oscillations for the twist angle of the local minima, already observed in the 12-pyr case, are also present for the 42-pyr COF with a shorter period and reduced amplitude, except for the one at 11 degrees. In fact, as the COF grows, more pyrene moieties interact with the substrate, and the ones farther from the center cover a longer arc when compared to the ones closer to the rotation center, thereby exploring the space of stacking arrangements with graphene faster, Fig. S4. Indeed, the number of minima progressively disappears with increasing diameters, and it is strongly reduced already in the 240-pyr case, Fig. 2(h), where only a slight wiggling in the energy is observed. This is due to the slight incommensurability between the COF and graphene lattices matching similar observations in incommensurate graphitic nanomaterials[39–41].

Relevantly, all curves share a feature at 11 degrees, Fig. 2(i), characterized by an energy minimum in the AA sampling point, whereas a maximum is found for the AB sampling point. Finally, in the 756-pyr case, which is large enough to reveal a complete moiré superlattice, Fig. 2(j), the periodic oscillations are mostly smoothed out, as the potential energy surface nearly flattens. However, the minimum at 11 degrees for the AA sampling point is still present, Fig. 2(i). This indicates that, in contrast with the periodic oscillations, this is not a size-dependent effect but rather an intrinsic feature shared by PDBA COFs of different sizes on graphene. In fact, an analysis of the local stacking reveals that most pyrene moieties of PDBA COFs twisted by 11 degrees are stacked in a staggered conformation with respect to the underlying graphene lattice and thus prevent forming a moiré pattern, Fig. S5. Confirming this, by keeping the orientation and displacing the COF by 1.4 Å to the AB sampling point, a maximum in the energy is obtained, as there are now eclipsed-like pyrene stacking arrangements with respect to the substrate, which are energetically unfavourable, Fig. 3.

These results demonstrate that the PDBA COFs on graphene possess a well-defined minimum at a consistent twist angle, 11 degrees, whose appearance is driven by the stacking arrangement between the COF pyrene units and the graphene substrate. Confirming this, a distinctive structural aspect of this twisted arrangement, that is the absence of a moiré pattern, matches the experimental observations on grown twisted PDBA COFs on HOPG[4], where a moiré superlattice is also not observed.

Diffusion energetics

To understand how the twist angle affects the growing COFs diffusion on graphite[4], we calculated the rigid translational potential energy surface (PES) of a 12-pyr, a 42-pyr and a 240-pyr COF on graphene at different twist angles, namely 0, 11 and 18 degrees (Fig. 4, additional twist angles are available in the SI, Figure S6). For untwisted COFs, the PES reproduces the substrate lattice symmetry, where the minimum corresponds to Bernal-like stacking of pyrene moieties onto graphene. There are six symmetry equivalent directions at 60 degrees for which

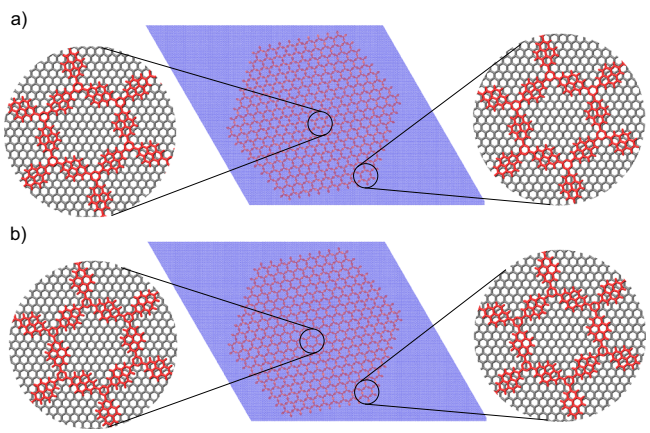

Fig. 3 | Local stacking at the 11-degree feature. Stacking arrangement of 756-pyr COF rotated by 11 degrees on graphene for the minimum energy **a** and maximum energy **b** stacking registries corresponding to the AA and AB sampling points, respectively.

https://doi.org/10.1038/s41467-025-67598-4

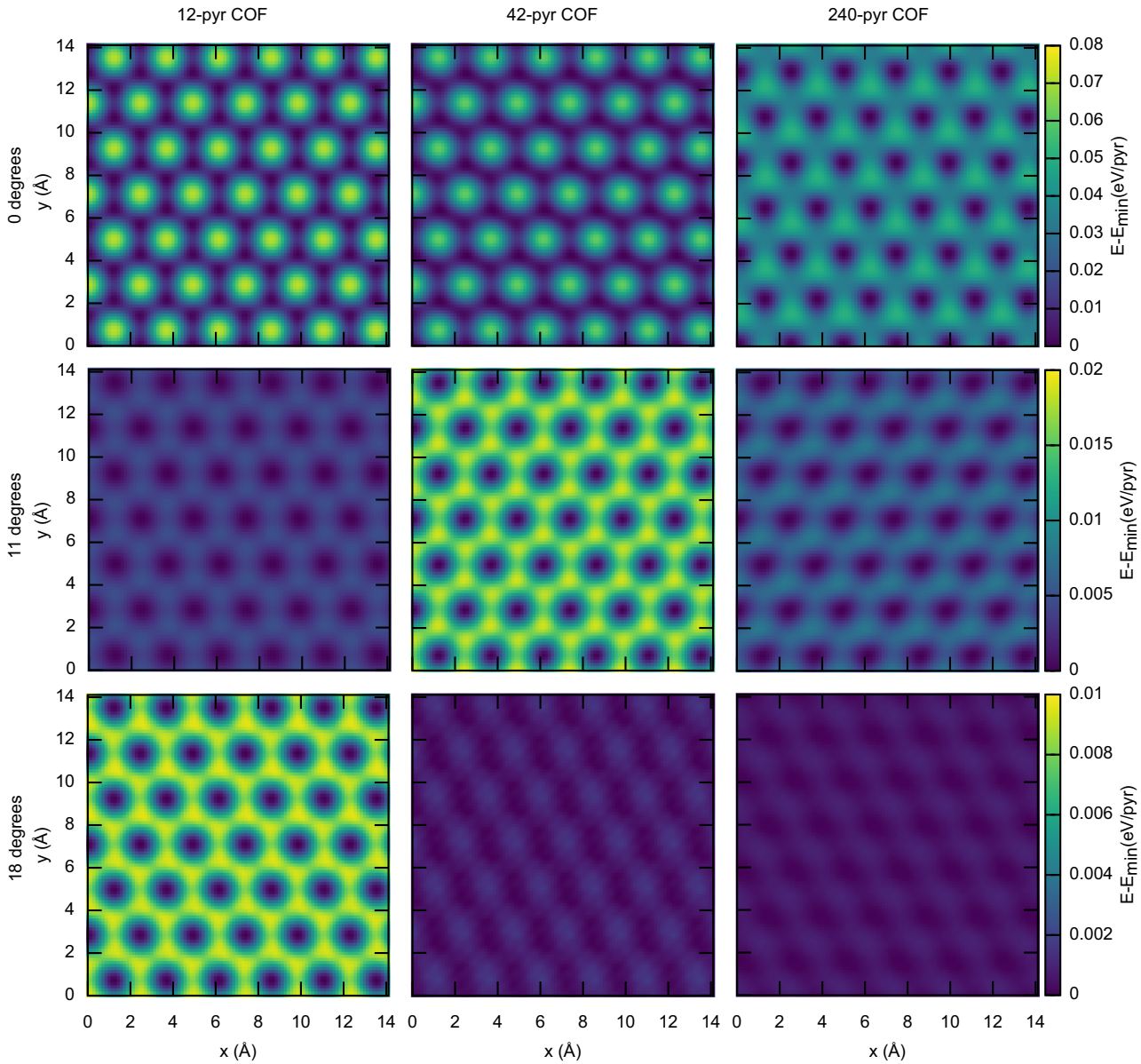

Fig. 4 | Diffusion at different twist angles. Potential Energy Surface (PES) for the 12-pyr (left column), the 42-pyr (center column) and the 240-pyr (right column) PDBA 2D-COFs on graphene at the twist angles of 0 (top), 11 (center) and 18 (bottom) degrees. Note the progressive flattening of the energy ranges for 11 and 18 degrees.

diffusion is most favourable, showing a barrier of 12 meV/pyr lying at the AA sampling points. There is no significant difference between the 12-pyr and 42-pyr case, except that the height of the maxima is slightly reduced in the latter. Interestingly, for the substantially larger 240-pyr COF, the energy barrier increases to 33 meV/pyr, and the number of minima is reduced by half.

When the twist angle between the COF and graphene is increased to 11 degrees, the PES gets shallower for the 12-pyr COF, with a sliding barrier of just 4 meV/pyr, indicating that at this orientation mobility is enhanced. Conversely, for the 42-pyr COF the sliding energy barrier increases to 15 meV/pyr, while the 240-pyr COF shows again a smaller barrier, 5 meV/pyr at the same twist angle. For a twist angle of 18 degrees, a barrier of 8 meV/pyr is present for the 12-pyr COF, while, for this case, the energy surface is virtually flat for the 42-pyr and 240-pyr.

These results, although static and thus indicative, reveal how the COF diffusivity is significantly affected by the twist angle and the COF size, and how, for certain angles, a dramatic impact on the barriers is expected. These, as already mentioned, are a clear effect of the COF/graphene lattices commensuration, which shows a strong dependence on size, especially for smaller COFs. In fact, as the COF size increases, the number of different stacking arrangements between the pyrene units and the substrate increases. This effect may translate into local stabilizing and destabilizing stacking geometries with their corresponding effects on the interaction energies and diffusion barriers. These factors should play a significant role during the growth of COFs at the reported experimental conditions[4], for instance, enhancing oriented particle attachment[42]. In this regard, twisted orientations with enhanced mobilities would not only be expected to have larger entropic contributions but might also facilitate the growth of extended high-quality twisted PDBA COFs on graphite[4,13].

Lattice mismatch variation

It is relevant to address how sensitive our findings are to changes in the commensurability of the COF and graphene lattices. To assess this, we computed the 240-pyr COF at the AA sampling point and explored the twisting energetics using a range of compressed and expanded graphene substrates, Fig. 5. The minimum at 11 degrees was found for strains between −1.5 % and 0.5 %, that is larger than the estimated error

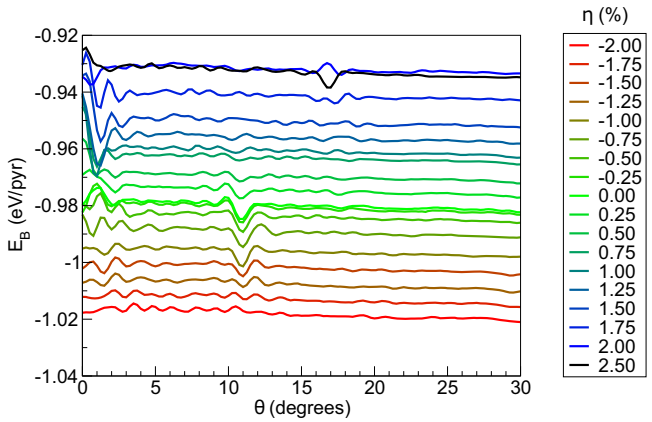

Fig. 5 | Twisting energetics with different lattice commensurabilities. Binding energies for different twist angles for a 240-pyr COF on compressed and expanded graphene substrates (see methods for details).

of the force field for lattice parameters versus DFT for PDBA COFs (about 0.3 %, Table 1). Interestingly, when a strain of 2.5 % is applied, a well-defined minimum appears at 17 degrees, better matching the experimental twist of PDBA monolayers grown on HOPG, 19 degrees[4]. This discrepancy may arise from a number of experimental factors which, for the sake of computational feasibility, were not present in our study. Dynamic and temperature effects, anharmonic vibrations, as well as solvent and other local environmental effects, may alter differently the graphene and PDBA lattices, potentially stabilising other twist angles. Relevantly, the presence of a unique twist angle lacking a moiré superlattices in grown twisted COFs on HOPG[4] matches our findings.

In conclusion, we modelled the binding and diffusion barriers of growing diameter COFs with an ad-hoc hybrid force field thoroughly validated against DFT calculations. The models reveal more complex energetics for smaller COFs, which progressively simplify as COFs grow. A twist angle of 11 degrees was consistently found throughout all the simulations. This is due to the local stacking interactions between pyrene moieties and the graphene substrate, as this angle avoids high-energy stacking typical of moiré superlattices, matching experimental observations. Furthermore, we have shown that different twist angles should be obtained with slight variations on the lattice mismatch.

The influence of the twist angle on the diffusion of COFs was also addressed, indicating an enhancement of the COF mobility for twisted heterostructures, which, through the growth kinetics of the COF monolayer, should also lead to twisted COFs on graphite. Altogether, these findings reveal the complex and rich behaviour of twisted graphene/COF heterostructures, addressing the different rules relevant to twist engineering these rather remarkable synthetic materials.

Methods

Molecular mechanics simulations were performed using LAMMPS[43]. The Yaff code[44] was used to assign the ReDD-COFFEE[23] (RC) force field parameters for the PDBA COF. For simplicity and computational efficiency, the graphite substrate[4] was represented with a periodic static graphene monolayer, on top of which non-periodic, pyrene-terminated PDBA COFs were deposited. To maximize symmetry and minimize undesirable energy variations, the edge pyrenes were capped with hydrogen in all cases. Comparative calculations with DFT and MM Hamiltonians with graphene and few-layer-graphene substrates yielded fundamentally equivalent results, Table S2 and Fig. S7.

The Dihedral-angle-corrected Registry-dependent Interlayer Potential (DRIP)[29] was used to treat the interactions between graphene and the pyrene moieties of the COF, while the interactions between the boroxine rings and the graphene substrate were treated using RC. Full periodic boundary conditions were used in all calculations via a slab model with a perpendicular dimension of at least 50 Å to minimize COF inter-cell interactions. To calculate the binding energy as a function of the twist angle in graphene/COF heterostructures, the COF was initially relaxed without twisting and then twisted around its center of mass in 0.25 degrees steps up to 30 degrees on the axis normal to the graphene plane. To allow for direct comparison, the substrate and COF orientations were chosen consistently with the experimental observations[4]. The binding energy was calculated as the difference between the graphene/COF energy and the energy of the same system in which the COF is vertically displaced by half unit cell (25 Å) and relaxed. In addition, to study graphene substrates with different COF commensurabilities, an equibiaxial strain η was imposed so that the graphene periodic cells were rescaled according to

$$a = a_0(1+\eta), \tag{1}$$

where a and a_0 are the strained and unstrained lattice parameters, respectively, so that a positive η value corresponds to a lattice dilatation.

DFT periodic calculations were performed with the PBE[45] functional augmented with Many Body Dispersion (MBD) corrections computed with FHI-aims[46–48] using "tight" numerical orbitals and a Γ-centered 3x3x1 k-point grid, following previous studies[49,50]. All systems were optimized with fixed cell angles with a maximal force threshold of 0.001 eV/Å. For visualization purposes, the code VMD[51] was used.

Data availability

Data required to reproduce the results described in this work is available from the authors upon request.

References

1. Colson, J. W. & Dichtel, W. R. Rationally synthesized two-dimensional polymers. *Nat. Chem.* **5**, 453–465 (2013).
2. Huang, N., Wang, P. & Jiang, D. Covalent organic frameworks: a materials platform for structural and functional designs. *Nat. Rev. Mater.* **1**, 1–19 (2016).
3. Colson, J. W. et al. Oriented 2D covalent organic framework thin films on single-layer graphene. *Science* **332**, 228–231 (2011).
4. Zhan, G. et al. Observing polymerization in 2D dynamic covalent polymers. *Nature* **603**, 835–840 (2022).
5. Wang, C. et al. A graphene-covalent organic framework hybrid for high-performance supercapacitors. *Energy Storage Mater.* **32**, 448–457 (2020).
6. Li, C. et al. Ultralight covalent organic framework/graphene aerogels with hierarchical porosity. *Nat. Commun.* **11**, 4712 (2020).
7. Xiong, Y. et al. Ultrahigh responsivity photodetectors of 2D covalent organic frameworks integrated on graphene. *Adv. Mater.* **32**, 1907242 (2020).
8. Weare, B. L. et al. Imaging and analysis of covalent organic framework crystallites on a carbon surface: a nanocrystalline scaly COF/nanotube hybrid. *Nanoscale* **13**, 6834–6845 (2021).
9. Ren, W. et al. Impact of moiré superlattice on atomic stress and thermal transport in van der Waals heterostructures. *Appl. Phys. Rev.* **10**, 041404 (2023).
10. Jiang, W., Ni, X. & Liu, F. Exotic TOpological Bands and Quantum States in Metal–organic and Covalent–organic Frameworks. *Acc. Chem. Res.* **54**, 416–426 (2021).
11. Kapfer, M. et al. Programming twist angle and strain profiles in 2D materials. *Science* **381**, 677–681 (2023).
12. Cao, Y. et al. Unconventional superconductivity in magic-angle graphene superlattices. *Nature* **556**, 43–50 (2018).
13. Zhan, G. et al. Moiré two-dimensional covalent organic framework superlattices. *Nat. Chem.* 1–7. https://doi.org/10.1038/s41557-025-01748-5 (2025).

14. Bistritzer, R. & MacDonald, A. H. Moiré bands in twisted double-layer graphene. *Proc. Natl. Acad. Sci.* **108**, 12233–12237 (2011).
15. Carr, S., Fang, S. & Kaxiras, E. Electronic-structure methods for twisted moiré layers. *Nat. Rev. Mater.* **5**, 748–763 (2020).
16. Jorgensen, W. L., Maxwell, D. S. & Tirado-Rives, J. Development and testing of the OPLS all-atom force field on conformational energetics and properties of organic liquids. *J. Am. Chem. Soc.* **118**, 11225–11236 (1996).
17. Rappe, A. K., Casewit, C. J., Colwell, K. S., Goddard, W. A. I. & Skiff, W. M. UFF, a full periodic table force field for molecular mechanics and molecular dynamics simulations. *J. Am. Chem. Soc.* **114**, 10024–10035 (1992).
18. Halgren, T. A. Merck molecular force field. I. Basis, form, scope, parameterization, and performance of MMFF94. *J. Comput. Chem.* **17**, 490–519 (1996).
19. Allinger, N. L., Yuh, Y. H. & Lii, J. H. Molecular mechanics. The MM3 force field for hydrocarbons. 1. *J. Am. Chem. Soc.* **111**, 8551–8566 (1989).
20. Vanommeslaeghe, K. et al. CHARMM general force field: a force field for drug-like molecules compatible with the CHARMM all-atom additive biological force fields. *J. Comput. Chem.* **31**, 671–690 (2010).
21. Schmid, R. & Tafipolsky, M. An accurate force field model for the strain energy analysis of the covalent organic framework COF-102. *J. Am. Chem. Soc.* **130**, 12600–12601 (2008).
22. Amirjalayer, S., Snurr, R. Q. & Schmid, R. Prediction of structure and properties of boron-based covalent organic frameworks by a first-principles derived force field. *J. Phys. Chem. C.* **116**, 4921–4929 (2012).
23. Vos, J. S. D., Borgmans, S., Voort, P. V. D., Rogge, S. M. J. & Speybroeck, V. V. ReDD-COFFEE: a ready-to-use database of covalent organic framework structures and accurate force fields to enable high-throughput screenings. *J. Mater. Chem. A* **11**, 7468–7487 (2023).
24. Zhang, T., Xue, Q., Zhang, S. & Dong, M. Theoretical approaches to graphene and graphene-based materials. *Nano Today* **7**, 180–200 (2012).
25. Strutyński, K., Melle-Franco, M. & Gomes, J. A. N. F. New parameterization scheme of DFT-D for graphitic materials. *J. Phys. Chem. A* **117**, 2844–2853 (2013).
26. Strutyński, K., Gomes, J. A. N. F. & Melle-Franco, M. Accuracy of dispersion interactions in semiempirical and molecular mechanics models: the benzene dimer case. *J. Phys. Chem. A* **118**, 9561–9567 (2014).
27. Kolmogorov, A. N. & Crespi, V. H. Registry-dependent interlayer potential for graphitic systems. *Phys. Rev. B* **71**, 235415 (2005).
28. Zhang, X., Chen, Z., Chen, H. & Xu, L. Comparative studies of thermal conductivity for bilayer graphene with different potential functions in molecular dynamic simulations. *Results Phys.* **22**, 103894 (2021).
29. Wen, M., Carr, S., Fang, S., Kaxiras, E. & Tadmor, E. B. Dihedral-angle-corrected registry-dependent interlayer potential for multilayer graphene structures. *Phys. Rev. B* **98**, 235404 (2018).
30. Li, H. & Kim, W. K. A comparison study between the Lennard-Jones and DRIP potentials for friction of graphene layers. *Comput. Mater. Sci.* **180**, 109723 (2020).
31. Hao, W. et al. Dynamic insights into the growth mechanisms of 2D covalent organic frameworks on graphene surfaces. *ACS Nano* **18**, 10485–10494 (2024).
32. Wang, Z. et al. Growth of two-dimensional covalent organic frameworks on substrates: insight from microsecond atomistic simulations. *Chem. Sci.* **15**, 17629–17641 (2024).
33. Naik, M. H., Maity, I., Maiti, P. K. & Jain, M. Kolmogorov–Crespi potential for multilayer transition-metal dichalcogenides: capturing structural transformations in Moiré superlattices. *J. Phys. Chem. C.* **123**, 9770–9778 (2019).
34. Huang, J. et al. Room-temperature stacking disorder in layered covalent-organic frameworks from machine-learning force fields. *Mater. Horiz.* **10**, 2883–2891 (2023).
35. Wen, M. & Tadmor, E. B. Hybrid neural network potential for multilayer graphene. *Phys. Rev. B* **100**, 195419 (2019).
36. Rowe, P., Deringer, V. L., Gasparotto, P., Csányi, G. & Michaelides, A. An accurate and transferable machine learning potential for carbon. *J. Chem. Phys.* **153**, 034702 (2020).
37. Zuo, Y. et al. Performance and cost assessment of machine learning interatomic potentials. *J. Phys. Chem. A* **124**, 731–745 (2020).
38. Ouyang, W., Mandelli, D., Urbakh, M. & Hod, O. Nanoserpents: graphene nanoribbon motion on two-dimensional hexagonal materials. *Nano Lett.* **18**, 6009–6016 (2018).
39. Kolmogorov, A. N. & Crespi, V. H. Smoothest bearings: interlayer sliding in multiwalled carbon nanotubes. *Phys. Rev. Lett.* **85**, 4727–4730 (2000).
40. Sinclair, R. C., Suter, J. L. & Coveney, P. V. Graphene–graphene interactions: friction, superlubricity, and exfoliation. *Adv. Mater.* **30**, 1705791 (2018).
41. Wang, J., Khosravi, A., Vanossi, A. & Tosatti, E. Colloquium: sliding and pinning in structurally lubric 2D material interfaces. *Rev. Mod. Phys.* **96**, 011002 (2024).
42. Li, D. et al. Direction-specific interactions control crystal growth by oriented attachment. *Science* **336**, 1014–1018 (2012).
43. Thompson, A. P. et al. LAMMPS—a flexible simulation tool for particle-based materials modeling at the atomic, meso, and continuum scales. *Computer Phys. Commun.* **271**, 108171 (2022).
44. Software | Center for Molecular Modeling. https://molmod.ugent.be/software.
45. Perdew, J. P., Burke, K. & Ernzerhof, M. Generalized gradient approximation made simple. *Phys. Rev. Lett.* **77**, 3865–3868 (1996).
46. Blum, V. et al. Ab initio molecular simulations with numeric atom-centered orbitals. *Computer Phys. Commun.* **180**, 2175–2196 (2009).
47. Marek, A. et al. The ELPA library: scalable parallel eigenvalue solutions for electronic structure theory and computational science. *J. Phys. Condens. Matter* **26**, 213201 (2014).
48. Yu, V. W. et al. ELSI — An open infrastructure for electronic structure solvers. *Computer Phys. Commun.* **256**, 107459 (2020).
49. Martínez-Abadía, M. et al. π-interpenetrated 3D covalent organic frameworks from distorted polycyclic aromatic hydrocarbons. *Angew. Chem. Int Ed. Engl.* **60**, 9941–9946 (2021).
50. Martínez-Abadía, M. et al. A wavy two-dimensional covalent organic framework from core-twisted polycyclic aromatic hydrocarbons. *J. Am. Chem. Soc.* **141**, 14403–14410 (2019).
51. Humphrey, W., Dalke, A. & Schulten, K. VMD: visual molecular dynamics. *J. Mol. Graph* **14**, 33–38 (1996).

Acknowledgements

This work was developed within the scope of the project CICECO Aveiro Institute of Materials, UID/50011/2025 (https://doi.org/10.54499/UID/50011/2025) & LA/P/0006/2020 (https://doi.org/10.54499/LA/P/0006/2020), financed by national funds through the FCT/MCTES (PIDDAC). We acknowledge the Laboratory for Advanced Computing at the University of Coimbra for providing HPC resources in the framework of the computational resources grant 2023.10530.CPCA.A2, V.L. and M.M.-F., provided by FCT (https://doi.org/10.54499/2023.10530.CPCA.A2). This project has received funding from the European Union's Horizon 2020 Research and Innovation Programme under Grant Agreements No. 101046231, M.M.-F. and K.S., and No. 958174 and from the Foundation for Science and Technology (FCT) under grant agreements M-ERA-NET3/0006/2021 (M.M.-F., K.S. and V.L.) and 2022.07534.CEECIND, K.S.

Author contributions

M.M.-F. and V.L. conceived the research. V.L. and K.S. developed and ran the computer models, supervised by M.M.-F. V.L. wrote the initial draft with the help of M.M.-F, and all authors contributed to further review and editing. All authors have approved the final version of the manuscript.

Competing interests

The authors declare no competing interests.

Additional information

Supplementary information The online version contains supplementary material available at https://doi.org/10.1038/s41467-025-67598-4.

Correspondence and requests for materials should be addressed to Manuel Melle-Franco.

Peer review information *Nature Communications* thanks Hongjun Lin, Mingchao Shao and the other anonymous reviewer(s) for their contribution to the peer review of this work. A peer review file is available.